



HAL
open science

Insights on the synthesis mechanism of green phenolic resin derived porous carbons via a salt-soft templating approach

Cristina Nita, Mahmoud Bensafia, Cyril Vaultot, Luc Delmotte, Camelia Matei Ghimbeu

► To cite this version:

Cristina Nita, Mahmoud Bensafia, Cyril Vaultot, Luc Delmotte, Camelia Matei Ghimbeu. Insights on the synthesis mechanism of green phenolic resin derived porous carbons via a salt-soft templating approach. *Carbon*, 2016, 109, pp.227-238. 10.1016/j.carbon.2016.08.011 . hal-02465100

HAL Id: hal-02465100

<https://hal.science/hal-02465100v1>

Submitted on 7 Feb 2020

HAL is a multi-disciplinary open access archive for the deposit and dissemination of scientific research documents, whether they are published or not. The documents may come from teaching and research institutions in France or abroad, or from public or private research centers.

L'archive ouverte pluridisciplinaire **HAL**, est destinée au dépôt et à la diffusion de documents scientifiques de niveau recherche, publiés ou non, émanant des établissements d'enseignement et de recherche français ou étrangers, des laboratoires publics ou privés.

Insights on the synthesis mechanism of green phenolic resin derived porous carbons *via* a salt-soft templating approach

Cristina Nita ^{a, b}, Mahmoud Bensafia ^{a, c}, Cyril Vaultot ^a, Luc Delmotte ^a,
Camelia Matei Ghimbeu ^{a, *}

^a *Université de Strasbourg, Université de Haute Alsace, Institut de Science des Matériaux de Mulhouse, CNRS UMR 7361, 15 rue Jean Starcky, 68057 Mulhouse, France*

^b *National Institute for Lasers, Plasma and Radiation Physics, Atomistilor 409 bis, RO-77125 Magurele, Romania*

^c *Université de Strasbourg, UFR Physique, 3-5 Rue de l'Université, F-67081 Strasbourg, France*

A B S T R A C T

A combined salt-soft template approach to synthesize porous carbon materials is reported along with their synthesis mechanism. This consists in the evaporation induced self-assembly (EISA) of aqueous solutions containing green phenolic resins, a triblock copolymer template and a metallic salt, followed by thermal treatment and washing. The increase of pH up to 5 using NaOH, induces significant improvement in the carbon microporosity but in the detrimental of mesoporosity. As suggest by ¹³C and ¹H NMR, the mesoporosity lost is caused by the decrease of H-bonding and self-assembly between the phenolic resin and the template due to the strong “salting-out” effect of –OH ions. For higher pH (pH-9), the porosity start to decrease and graphene-sheet like morphology is formed. The microporosity varies with the salt in the following order: KCl > NaCl > LiCl, while the mesoporosity in the opposite way. The structure changes as well from smooth turbostatic (KCl) to defective graphitic one (NaCl, LiCl). These textural and structural modifications are explained in terms of cation hydration enthalpy and cation- π binding energy and by the competition between the metal salt cations and the Na ions (used to regulate the pH) for water or phenolic resin aromatic ring sites.

1. Introduction

Porous carbon materials are widely used in many fields of applications such as gas adsorption and separation, catalysis, water purification and energy storage [1–6]. Particularly, ordered mesoporous carbons (OMC) become very attractive owing to their controlled uniform pore size distribution, pore connectivity and large variety of pore and particle morphology [4]. The design of such materials can be achieved mainly by two synthetic approaches, i.e., hard-template (nanocasting) or soft-template. In the hard-template approach, a mesoporous silica template is usually used and infiltrated by a carbon precursor followed by thermal treatment and etching of silica with strong acids or bases [7–9]. The multistep reaction synthesis involving hazardous products is regarded as a limitation of this approach. Therefore, the soft-template method, more recently developed, seems more

promising due to the limited steps involved, easiness of preparation and large choice of synthesis parameters allowing to obtain carbon materials with various features [10–12]. In such approach, thermosetting phenolic resins are self-assembled with an amphiphilic triblock copolymer template *via* hydrogen or covalent bonding. A thermal treatment allows to decompose the phenolic resin and the template leading to the formation of a mesoporous carbon. Usually, phenol-formaldehyde resins are employed as carbon source in majority of published works [11], even if they are known to be carcinogen. Recently, we have proposed as a substituent of formaldehyde, a plant derived aldehyde, i.e., glyoxylic acid, which play a role of cross-linker and catalyst due to its double functionality (aldehyde/carboxylic acid), hence, the use of strong acids is not longer required as well [13]. Despite the large pallet of parameters that can be varied in soft-template approach, carbon materials with specific area higher than ~700–800 m²/g is still difficult to achieve, and, in the same time, very challenging [14–18].

Several ways were proposed to overcome this inconvenient. Firstly, the classical activation route of carbon in gas phase (H₂O

vapor, CO₂) or with chemical reagents (KOH, H₃PO₄ ...) may be used with success and, in some cases, the mesoporosity may be even preserved [19,20]. The main limitation of such route is related to the consumption of carbon, hence the low yield of reaction. Alternative ways to improve the surface area by using supplementary sacrificial template such as colloidal silica or by employing laboratory made templates have been also reported [21–24].

Recently, a salt-template route was proposed by Mokaya and Antonietti [25,26] for the preparation of micro/mesoporous materials. A carbon source is mixed with a salt followed by thermal treatment and washing to remove the salt template. The advantage of such method is motivated by the use of cheap salts, which can be in addition recovered in the end of synthesis, but also by the high yield of obtained carbon compared with activation routs. Mostly, inorganic salt were used (KCl, LiCl, CaCl₂, ZnCl₂, NaCO₃ or their mixture), but some works using organic salt (potassium oxalate) were as well reported [26]. As carbon source, glucose was the most employed, but ionic liquids, phenolic resins or chitosan were used as well [25–32]. The increase of the temperature and the amount of salt prove to be important parameters to increase the carbon textural features. Therefore, materials with developed microporosity/mesoporosity up to 2100 m² g⁻¹ specific surface area and 1.5 cm³ g⁻¹ porous volumes could be obtained [30]. By combining the salt template with hard template approach, impressive total porous volume (up to 4.3 cm³/g) could be reached as well [27]. However, in none of these works the synthesis mechanism was discussed.

The aim of this paper is to combine the salt and soft template approaches in order to obtain high surface area carbon materials with various textural features. A second goal is to understand the synthesis mechanism of self-assembly of phenolic resins in the presence of organic templates, alkaline salts and bases and their effects on the textural, structural and morphological features of derived carbons. To our knowledge, such complex synthesis mechanisms were not addressed up to now. For this aim, green phenolic resins based on phloroglucinol/glyoxylic acid are employed together with a triblock polymer template to create the mesoporosity and several salts (KCl, NaCl and LiCl) to improve the microporosity. The influence of type of salt, pH of the solution and thermal treatment temperature on the carbon and phenolic resins characteristics were studied in detail. A synthesis mechanism is proposed based on ¹³C and ¹H NMR at high and low fields, TGA and TEM analysis.

2. Experimental part

2.1. Material synthesis

Triblock copolymer Pluronic F127 [poly (ethylene oxide)-blockpoly(propylene oxide)-*block*-poly-(ethylene oxide, PEO₁₀₆P-PO₇₀PEO₁₀₆, Mw = 12,600 Da)], phloroglucinol (1,3,5-benzotriol, C₆H₆O₃), glyoxylic acid monohydrate (C₂H₂O₃·H₂O), absolute ethanol (C₂H₆O), potassium chloride (KCl), sodium chloride (NaCl) and lithium chloride (LiCl) were purchased from Sigma-Aldrich. Carbon materials were prepared by soft-template method involving phloroglucinol and glyoxylic acid as carbon precursors with a triblock copolymer template Pluronic F127, followed by thermal treatment. In a typical synthesis, phloroglucinol (0.83 g), glyoxylic acid (0.78 g) and pluronic F127 (1.6 g) were dissolved at room temperature in 10 ml of ethanol, followed by the addition of 20 ml of water. Then, the KCl metallic salt was dissolved in 10 ml of water, added in the first solution and further mixed together for 30 min. The molar ratio between the phenolic resin and the salts was kept to 1:2. The pH of the obtained

solution was ~1 and was tuned up to 9 using aqueous NaOH solution (1.25 M). The as obtained solutions were casted into Petri dishes and evaporated in a fume-hood for 12 h according to the EISA method (evaporation induced self-assembly). Thermopolymerization was performed at 120 °C, for 12 h, followed by a thermal treatment under argon up to 900 °C during 1 h (2 K/min slope). The KCl salt was removed by washing with hot distilled water (90 °C, 4 h). The influence of several metallic salts (NaCl, KCl and LiCl), of pH (1, 3, 5 and 9), of thermal treatment temperature (600 °C, 750 °C and 900 °C) on the carbon and phenolic resins materials characteristics was studied. Considering the complex reaction mixture, in order to discriminate between the effect of each component, several materials have been prepared in the absence of: salt (No salt), template (pH-1 NT, pH-5 NT), NaOH (pH-1), salt and NaOH (pH-1 NS). All synthesis parameters used are listed in Table 1 along with the nomination of the obtained corresponding materials.

2.2. Material characterization

Carbon textural properties were measured by nitrogen adsorption at 77 K using a Micromeritics ASAP 2420 instrument. Prior to the analysis, the materials were degassed overnight in vacuum at 300 °C. The BET specific surface area (SSA) was calculated from the linear plot in the relative pressure range of 0.01–0.05. The micropore volume (V_{micro}) was obtained using the Dubinin-Radushkevich (DR) equation in the relative pressure interval (P/P₀) from 10⁻⁴ to 10⁻². The total pore volume (V_T) was determined from the amount of nitrogen adsorbed at a relative pressure of 0.99. The mesoporous volume (V_{meso}) was determined by subtracting the microporous volume from the total pore volume. The pore size distributions (PSD) were determined from the adsorption branch of nitrogen isotherms using the 2D NLDFT heterogeneous surface model for carbon materials implemented in SAIEUS (Micromeritics) [33,34]. The carbonaceous material morphology was evaluated by TEM with a JEOL, ARM-200F model instrument operating at 200 kV. The long-range ordering of the materials was studied by small angle X-Ray scattering (SAXS) analysis by a Rigaku SMax 3000 equipped with a rotating Cu anode Micromax- 007HF (40 kV, 30 mA) and OSMIC CMF optics. Raman measurements were

Table 1
Synthesis conditions used for the preparation of carbon materials.

Material	pH	Temperature	Salt	NaOH	Template
pH-1 NS	1	900 °C	No	No	Yes
pH-1	1	900 °C	KCl	No	Yes
pH-3	3	900 °C	KCl	Yes	Yes
pH-5	5	900 °C	KCl	Yes	Yes
pH-9	9	900 °C	KCl	Yes	Yes
No salt	5	900 °C	–	Yes	Yes
KCl	5	900 °C	KCl	Yes	Yes
NaCl	5	900 °C	NaCl	Yes	Yes
LiCl	5	900 °C	LiCl	Yes	Yes
KCl-600	5	600 °C	KCl	Yes	Yes
KCl-750	5	750 °C	KCl	Yes	Yes
KCl-900	5	900 °C	KCl	Yes	Yes
LiCl-600	5	600 °C	LiCl	Yes	Yes
LiCl-750	5	750 °C	LiCl	Yes	Yes
LiCl-900	5	900 °C	LiCl	Yes	Yes
pH1-NT	1	900 °C	KCl	No	No
pH5-NT	5	900 °C	KCl	Yes	No

performed at room temperature in a backscattering geometry using a LabRAM BX40 (Horiba Jobin-Yvon) microspectrometer equipped with a He–Ne excitation source (wavelength 532 nm). The phenolic resin structure and the interactions with the template were studied by solid-state ^{13}C and ^1H magic angle spinning (MAS). NMR spectra were obtained at a frequency of 100.6 MHz, 400.13 MHz respectively on a Bruker Avance 400 NMR spectrometer. Supplementary details about the analysis may be found in the SI part. ^1H NMR relaxation experiments were performed for static samples in 9 mm NMR tubes on a Bruker Minispec MQ-20 spectrometer operating at a proton resonance frequency of 20 MHz. T_1 experiments were carried on by inversion recovery sequence.

3. Results

3.1. Carbon characterization

3.1.1. Influence of pH

The synthesis of carbon materials involves the self-assembly of green phenolic resin based on phloroglucinol/glyoxylic acid with a Pluronic F127 amphiphilic template in aqueous predominant medium. When the KCl is added in the mixture, the pH of overall solution is around ~ 1 . The obtained carbon using such solution (pH-1) is characterized by a type I/IV nitrogen adsorption/desorption isotherm (Fig. 1a) corresponding to a micro/mesoporous material. The high increase of adsorbed nitrogen amount in the low relative pressure region is associated with the formation of micropores induced by decomposition of phenolic resin. The observed H3 type hysteresis at higher relative pressures is related to the self-assembly of phenolic resin/template in macromolecular structure and further decomposition of the template with mesoporosity formation. The specific surface area is $538\text{ m}^2\text{ g}^{-1}$ while the microporous and mesoporous volume are 0.21 and $0.31\text{ cm}^3\text{ g}^{-1}$, respectively (Table 2). The pore size distribution (Fig. 1b) shows micropores centered on 0.6 nm and mesopores located around

Table 2

Textural characteristics of carbon materials obtained using different synthesis conditions.

Material	SSA $\text{m}^2\text{ g}^{-1}$	$V_T\text{ cm}^3\text{ g}^{-1}$	$V_{\text{micro}}\text{ cm}^3\text{ g}^{-1}$	$V_{\text{meso}}\text{ cm}^3\text{ g}^{-1}$
pH-1 NS	535	0.37	0.20	0.17
pH-1	538	0.52	0.21	0.31
pH-3	911	0.46	0.36	0.10
pH-5	1673	0.84	0.64	0.20
pH-9	1557	0.76	0.60	0.16
No salt	109	0.04	0.04	0.00
KCl	1673	0.84	0.64	0.20
NaCl	1449	0.75	0.55	0.20
LiCl	1150	0.81	0.43	0.38
KCl-600	1005	0.48	0.39	0.09
KCl-750	1383	0.64	0.54	0.10
KCl-900	1673	0.78	0.64	0.14
LiCl-600	567	0.41	0.23	0.18
LiCl-750	775	0.50	0.32	0.18
LiCl-900	1150	0.81	0.43	0.38
pH1-NT	752	0.31	0.30	0.01
pH5-NT	1815	0.76	0.73	0.03

SSA-total specific surface area determined by the BET method.

V_T , V_{micro} and V_{meso} - total pore volume, micropore volume and mesopore volume.

$7\text{--}8\text{ nm}$. The specific surface area and the microporous volume of pH-1 material are similar to that of carbon prepared in the absence of KCl (pH-1 NS), however, the mesoporous volume is higher (see Table 2). This comparison (pH-1 and pH-1 NS) suggests that the KCl salt do not allow improving the microporosity in such conditions, therefore, the influence of pH was further investigated.

For pH comprised between 3 and 9, the hysteresis shape changes from type H3 to H4 type. When the pH increases from 1 to 3, an increase of the specific surface area from $538\text{ m}^2\text{ g}^{-1}$ to

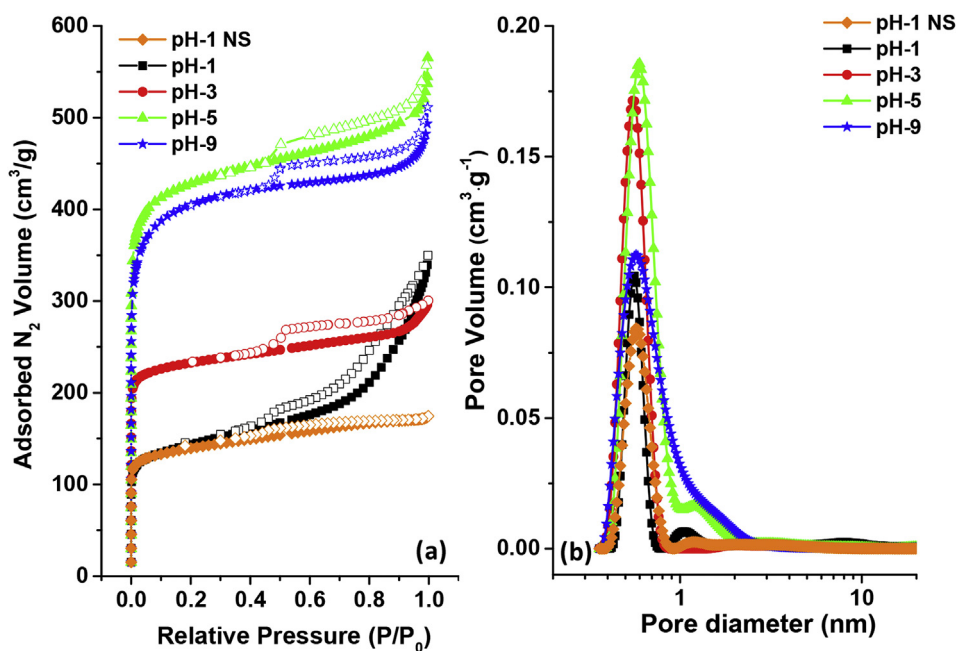


Fig. 1. Nitrogen adsorption/desorption isotherms (a) and 2D-NLDFT pore size distribution (b) of carbon materials synthesized using different pH of initial solutions: pH-1, pH-3, pH-5 and pH-9 (salt: KCl, T: $900\text{ }^\circ\text{C}$). For comparison reasons the isotherm and the pore size distribution for a carbon prepared at pH-1 in the absence of KCl salt is presented as well (pH-1 NS). (A color version of this figure can be viewed online.)

911 $\text{m}^2 \text{g}^{-1}$ is obtained. The microporous volume is mainly improved from 0.21 to 0.36 $\text{cm}^3 \text{g}^{-1}$ in the detriment of mesoporous volume which diminishes from 0.31 to 0.10 $\text{cm}^3 \text{g}^{-1}$. Further increase of the pH to 5 allows to better improve the microporosity (0.64 $\text{cm}^3 \text{g}^{-1}$) and the surface area (1673 $\text{m}^2 \text{g}^{-1}$) (Table 2). However, if higher pH is used, the SSA and the porous volumes slightly decrease; a slight increase in the micropore size distribution may be observed as well with the pH increase (Fig. 1b).

The morphology of the materials obtained with different pH conditions was as well examined. The TEM pictures of pH-1 material show an ordered hexagonal structure with parallel carbon channels and visible mesoporosity (Fig. 2a), in line with the adsorption results. The increase of the pH to 3 induces the formation of a disordered worm-like mesostructure (Fig. 2b) which disappears in the favor of a smooth microporous structure for pH-5 (Fig. 2c). Interestingly, when the pH is 9 (Fig. 2d) porous sheets of carbon with graphitic/graphene aspect are obtained. Raman spectra performed in several places on this sample (see Fig. S1, Supporting Informations) show a disordered structure (D peak is higher than G peak), but also the presence of the G' peak which originates from the staking of graphene sheets along the c -axis [35]. Hence, the pH greatly influences the textural, morphological and structural characteristics of derived carbons.

3.1.2. Influence of type of salt

As previously showed, the type of salt may alter the microporosity of the resulting carbon materials [25,27–32]. In the case of the soft-template synthesis, the salt modifies also the critical micellar concentration of the surfactant and, therefore, the self-assembly process and the polymerization rate of the phenolic resin.

Three salts were studied: KCl, NaCl and LiCl and the pH-5 allowing the obtain the highest surface area was selected. For comparison purposes one material was synthesized in the absence of any salt (No salt). The nitrogen adsorption/desorption isotherms and the pore size distribution of derived carbons are shown in Fig. 3.

When KCl and NaCl are used the isotherms are rather similar,

while in the case of LiCl a lower adsorbed nitrogen quantity is noticed in the low relative pressure region. The surface areas are: 1673, 1449 and 1150 $\text{m}^2 \text{g}^{-1}$ for KCl, NaCl and LiCl derived materials, respectively (Table 2). The microporosity increases, therefore, in the following order KCl > NaCl > LiCl, while the mesoporosity have an opposite behavior (see Table 2). If no salt is used, the textural properties are very low, a surface of only 109 $\text{m}^2 \text{g}^{-1}$ is reached.

This suggests on one hand that the salt play an important role on textural properties. On the other hand, if we compare the SSA of “no salt” material prepared in the absence of NaOH (109 $\text{m}^2 \text{g}^{-1}$) with that of material obtained in acidic conditions, hence in the absence of NaOH (pH-1 NS, 535 $\text{m}^2 \text{g}^{-1}$), lower textural properties are induce by the presence of NaOH. Therefore, basic conditions are not favorable for the self-assembly of the phenolic resin with the template. The micropore size is mainly centered on 0.6 nm as seen in Fig. 3b.

In the absence of salt, the morphology (Fig. 4a) shows some irregular mesopores. In the case of KCl the morphology is smooth (Fig. 4b), while for the NaCl and LiCl a sheet-like morphology is obtained (Fig. 4c–f).

Further insights on the carbon structure vs. the metal salt were assessed by Raman spectroscopy (Fig. 5). Several Raman spectra were taken in different zones of the materials and they present different ratio between the peak intensities or widths, suggesting heterogeneous structure in agreement with the TEM morphology. For clarity reasons, one representative spectrum for each material is shown (Fig. 5).

For KCl, the spectra are characterized by two peaks placed at 1325 cm^{-1} and 1590 cm^{-1} which correspond to the D (defects) and G (Csp^2 graphite) bands, respectively. When NaCl is used, the peaks become narrow and a third peak placed at 2640 cm^{-1} appears which is related to the G' band in graphite/graphene materials [36]. For LiCl the spectra looks similar to those of NaCl. For all materials the G band is more intense than the D band indicating a certain degree of structural ordering. The absence of G' band and the broader peaks in KCl materials may lead to the conclusion that it

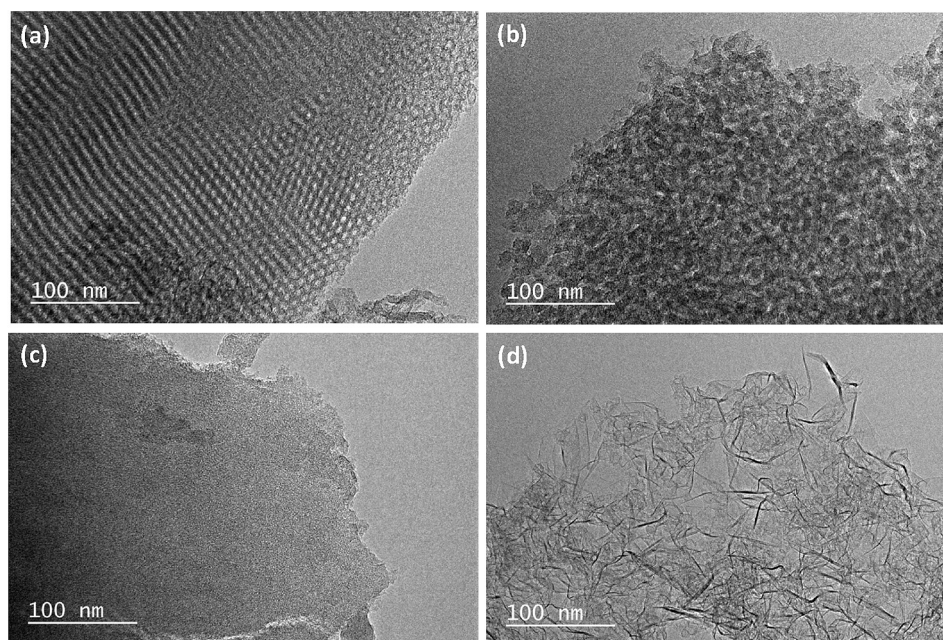


Fig. 2. TEM pictures of carbon materials synthesized using different pH of initial solutions: (a) pH-1; (b) pH-3; (c) pH-5 and (d) pH-9 (salt: KCl, T: 900 °C).

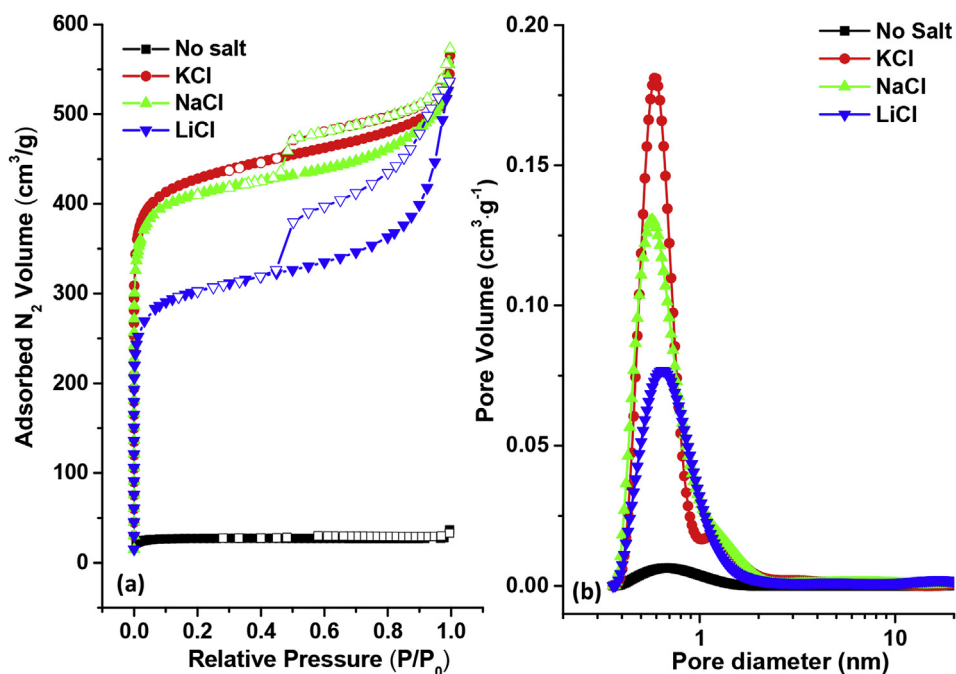


Fig. 3. Nitrogen adsorption/desorption isotherms (a) and 2D-NLDFT pore size distribution (b) of carbon materials synthesized using different salts: KCl, NaCl and LiCl or in the absence of salt; (pH-5, T: 900 °C). (A color version of this figure can be viewed online.)

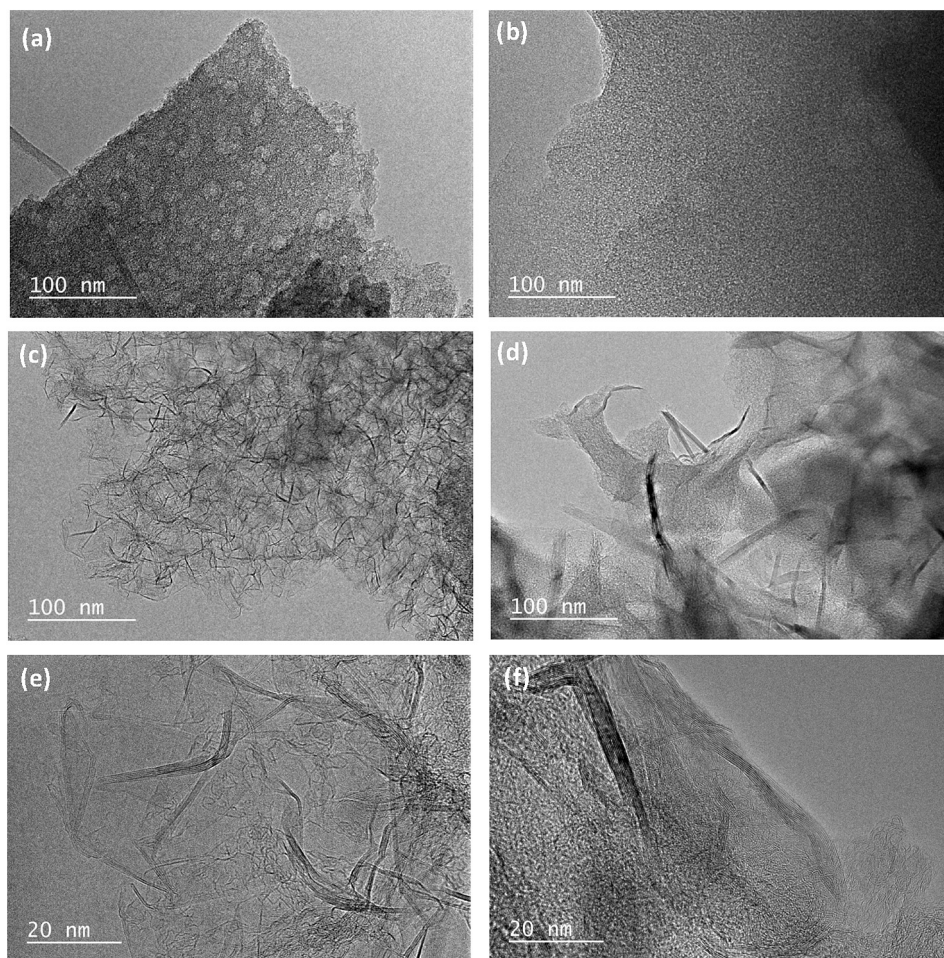


Fig. 4. TEM pictures of carbon materials synthesized (a) in the absence of salt or using different type of salts (b) KCl (c) NaCl and (d) LiCl and HRTEM of (e) NaCl and (f) LiCl carbons.

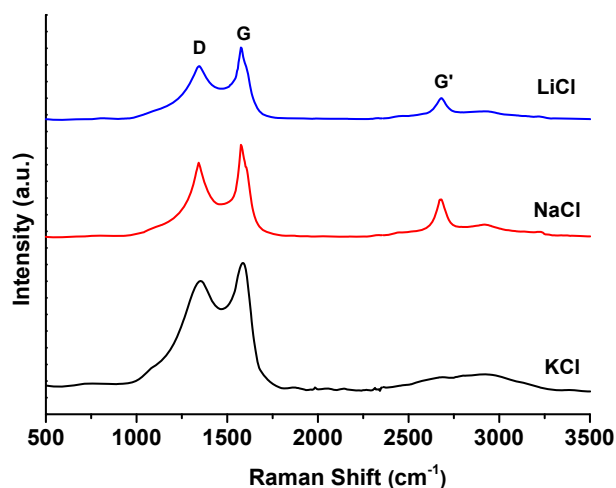


Fig. 5. Raman spectra of carbon materials synthesized in the presence of (a) KCl; (b) NaCl and (c) LiCl (pH-5; T: 900 °C). (A color version of this figure can be viewed online.)

exhibits the most disordered structure.

3.1.3. Influence of thermal treatment temperature

The influence of the thermal treatment temperature (600 °C, 750 °C and 900 °C) on the textural and structural properties of carbon materials was evaluated. Two salts giving significantly differences between textural properties at pH-5 (see Table 2) were selected for this study, i.e., KCl and LiCl. The nitrogen adsorption/desorption isotherms along with their pore size distribution are depicted in Fig. 6.

All materials prepared with KCl exhibit a type I isotherm (Fig. 6a) according to the IUPAC classification, characteristic to microporous materials. The increase of the thermal treatment

temperature from 600 °C to 900 °C induces an increase in the adsorbed nitrogen quantity and consequently of the specific surface area and microporous volume, from 1005 to 1673 m² g⁻¹ and from 0.39 to 0.64 cm³ g⁻¹, respectively. In addition, with the increase of the temperature some larger micropores (1.2 nm) are formed beside those at 0.6 nm (*in-set* Fig. 6a). Similar behavior was reported in other works using CaCl₂ or ZnCl₂ salts [26,28]. The mesopore volume is not varying up to 750 °C, and then an increase is observed for 900 °C, from 0.10 to 0.14 cm³ g⁻¹. The morphology is not changing with the temperature increase as demonstrated by TEM analysis (Fig. S2, SI).

The nitrogen adsorption/desorption isotherms for LiCl derived materials (Fig. 6b) show different shape compared to KCl, i.e. type I/IV which is characteristic to micro/mesoporous materials. However, the same evolution of textural vs. temperature as for KCl is observed, i.e., increase of the microporosity and mesoporosity with the temperature. The micropores sizes are centered around 0.6 nm (*in-set* Fig. 6b) while the mesopores around 50 nm as demonstrated by BJH pore size distribution (Fig. S3, SI). For LiCl, the temperature has an effect on the morphology/structure as well (see Fig. S4, SI). By increasing the temperature to 750 °C, graphitic-like sheets start to be formed as highlighted by TEM pictures and SAED (selected-area electron diffraction).

3.1.4. Influence of pluronic template

The influence of pluronic template presence/absence in the synthesis mixture on the textural/structural properties at pH 1 and 5 was investigated as well and the nitrogen adsorption/desorption isotherms are depicted in Fig. 7. In both pH cases, the presence/absence of template do not significantly modifies the nitrogen adsorption in the low relative pressure region related to the micropores.

The use of the template plays an important role on the mesoporosity. In the case of pH-1, a hysteresis associated with the condensation in the mesopores is observed (Fig. 7a). The mesoporous volume is significantly reduced from 0.31 to 0.20 cm³ g⁻¹

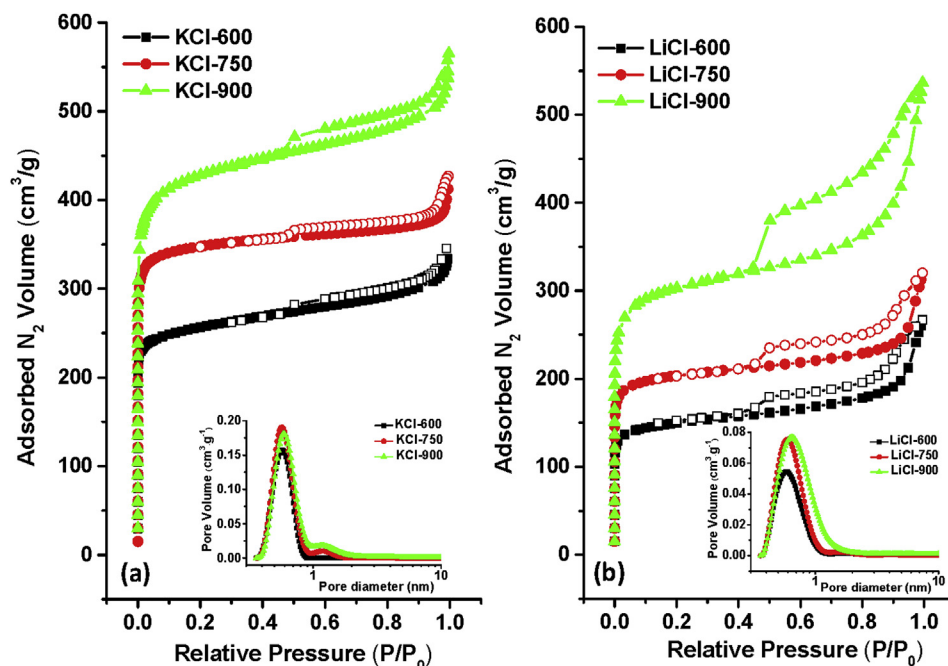


Fig. 6. Nitrogen adsorption/desorption isotherms of carbon materials synthesized using different temperatures 600 °C, 750 °C and 900 °C and different salts (a) KCl and (b) LiCl (pH-5); *in-set*: the corresponding 2D-NLDFT pore size distribution. (A color version of this figure can be viewed online.)

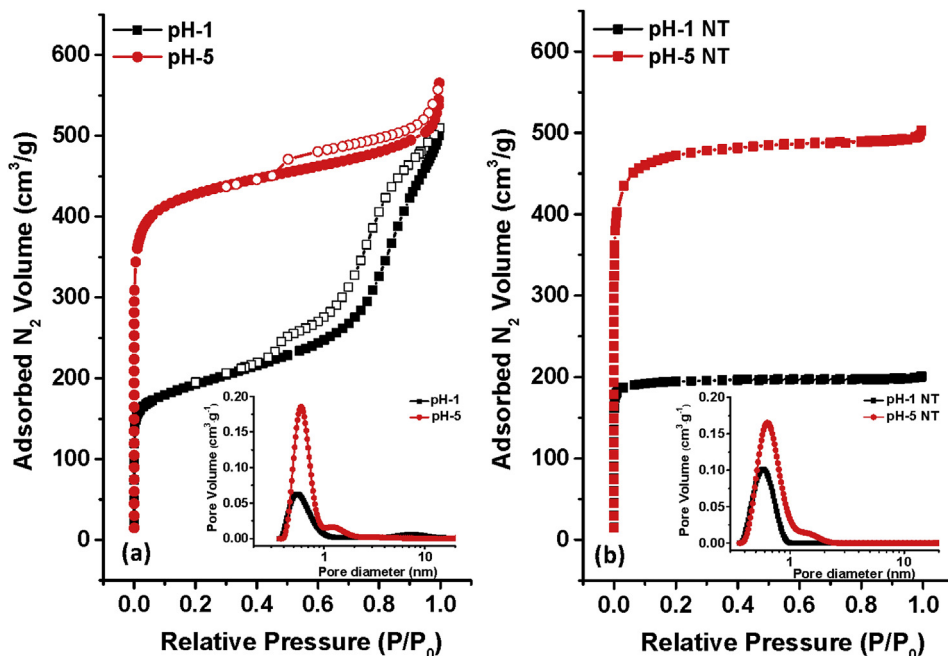


Fig. 7. Nitrogen adsorption/desorption isotherms of carbon materials synthesized using pH –1 and 5 in the presence of the template (a) and in the absence of the template (b) (salt KCl, T: 900 °C); *in-set*: the corresponding 2D-NLDFT pore size distribution. (A color version of this figure can be viewed online.)

when the pH increases from 1 to 5. This can be also visualized on the TEM pictures provided in Fig. S5, Supporting Informations.

In the absence of the template, perfectly type I isotherm specific to microporous materials with uniform small pore size distributions are obtained for pH 1 (Fig. 7b and *in-set*), while for pH-5 some larger micropore start to form (Fig. 7b and *in-set*). The specific surface area and the microporous volumes are slightly higher in the absence of the template, i.e. 1815 vs. 1673 m² g⁻¹ for pH5-NT and pH-5, respectively (Table 2).

In order to understand the formation of the microporosity/mesoporosity the thermopolymerized phenolic resins were analyzed.

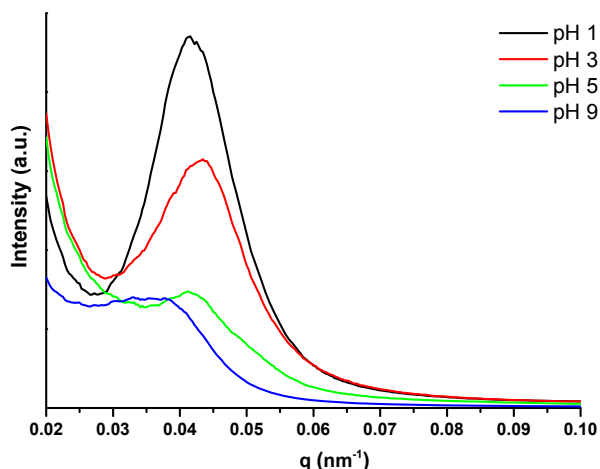


Fig. 8. (a) SAXS patterns of thermopolymerized phenolic resins prepared using different pH (salt KCl, time: 1 h). (A color version of this figure can be viewed online.)

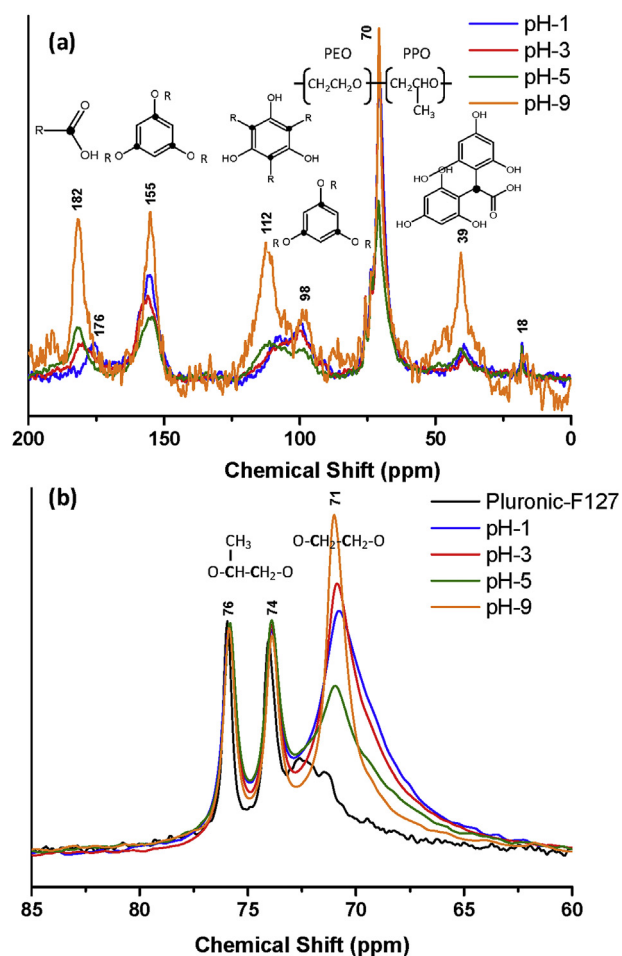
3.2. Characterization of the phenolic resin

The images of petri dishes containing phenolic resins obtained with various pH, dried at room temperature and further thermopolymerized at 120 °C are illustrated in Fig. S6 (Supporting Information). We can noticed that the color of the phenolic resin gradually shifts from colorless to dark orange when the pH changes from 1 to 9 (Fig. S6a–d). When the phenolic resins are thermopolymerized the color become dark-red no matter the pH used (Fig. S6e). This indicates oxidation of –OH groups and/or improve of crosslinking [37,38].

The SAXS patterns performed on thermopolymerized phenolic resins obtained with different pH conditions are shown in Fig. 8. One resolved peak placed at $q = 0.05 \text{ nm}^{-1}$ which corresponds to the 10 diffraction planes of an ordered 2D hexagonal p6m mesostructure [39] is observed. The peak intensity decreases progressively with the increase of the pH from 1 to 9, indicating the loss of mesoporosity ordering. This observation is in line with the TEM results on carbon materials (Fig. 2).

Further information about the structure of phenolic resins was assessed by solid state ¹³C and ¹H NMR (Figs. 9 and 10). The ¹³C CP-MAS (cross-polarization magic angle spinning) NMR spectra for pH-1 reveal several resonance peaks as seen in Fig. 9a. For more details, the assignments of NMR peaks are listed in Table S1 (Supporting Information). The most intense peak is placed at ~70 ppm and can be attributed to the carbon atoms bonded with O atoms (CH₂–O–CH₂) in the PEO moieties of copolymer template Pluronic F127 [40]. The other less intense proximity peaks from 74 -76 ppm and from 18 ppm are corresponding to the carbons involved in ethyl (–CH–CH₂) and methyl (–CH₃) groups, respectively, of the PPO moieties of Pluronic F127 template [41].

Several peaks placed at 176, 155, 109, 98 and 39 ppm are related to the carbons involved in the phenolic resins formed *via* the polymerization reactions between the phloroglucinol and glyoxylic acid. More precisely, they can be assigned to the several structures labeled as A, A' and B in Eq. (2). As described in detail before [13] in



the first stages of reaction, the phloroglucinol and the glyoxylic acid react giving rise to the so-called trihydroxy phenylacetic acid (see Eq. (1)). The structures A and A' are obtained *via* an electrophilic aromatic substitution reaction taking place between the trihydroxy phenylacetic acid and the phloroglucinol. Carboxylic acid bridges between the benzene rings are created and subsequent elimination of H₂O molecules through the condensation of the carboxylic and hydroxyl group allow the formation of lactone groups and therefore, the A, A' tautomeric structures (Eq. (2)). The reaction between the trihydroxy phenylacetic acid and the phloroglucinol may also lead to structure B (Eq. (2)).

When the pH increases from 1 to 9, the modification of peak intensity or/and position is clearly noticed. The peaks from 176 ppm corresponding to the carbon atoms bonded with O in carboxylic acid group, shift to higher resonances (182 ppm). This may be explained by the formation of R-COONa (K) species by deprotonation reactions of carboxylic acids groups in the presence of NaOH, which are known to shift the ¹³C NMR position. In addition, for pH-9 significant increase in the intensity of 176 ppm peak, as well as of the other peaks (155, 112, 98 and 39) is observed. This maybe related to an increase of the cross-linking of polymer chains *via* the formation of highly substituted phloroglucinol compounds and other polymeric structures as discuss further.

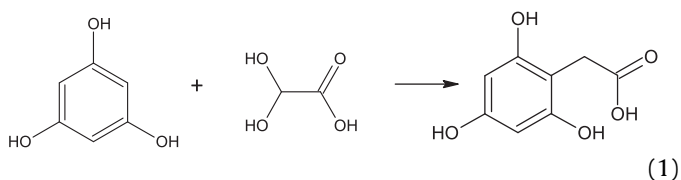
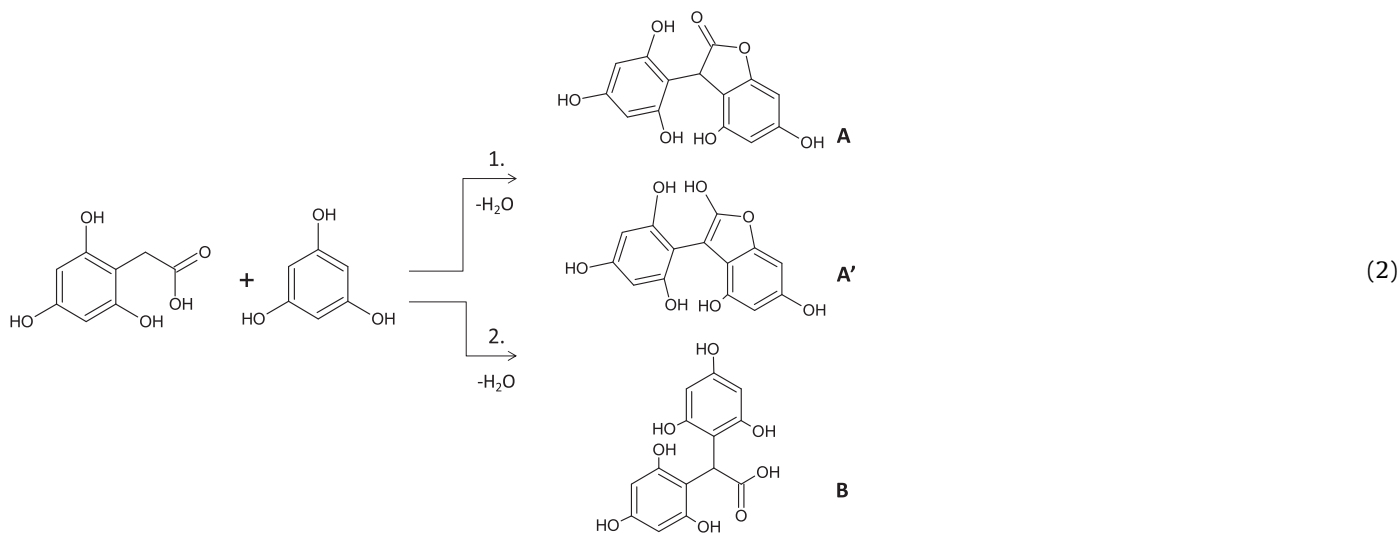


Fig. 9. (a) ¹³C CP-MAS and (b) ¹³C MAS-DEC solid-state NMR spectra of phenolic resins prepared using different pH conditions (salt KCl). (A color version of this figure can be viewed online.)



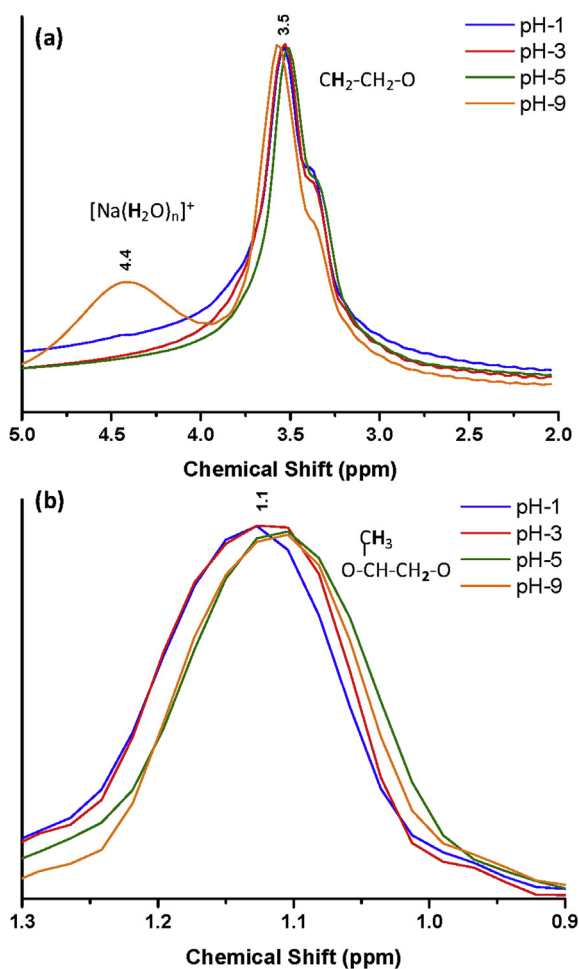
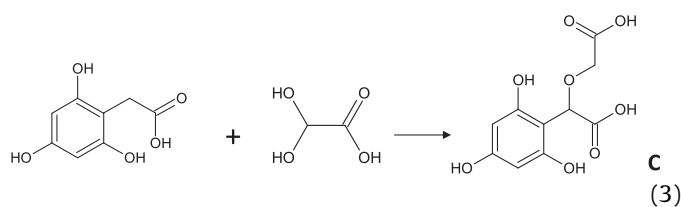


Fig. 10. ^1H solid state NMR spectra of phenolic resins prepared using different pH conditions (salt KCl). (A color version of this figure can be viewed online.)



As the CP-MAS NMR is a technique very sensitive to rigid carbons (phloroglucinol-glyoxylic acid based phenolic resin), we further performed MAS-DEC (magic angle spinning decoupling) spectra to get more insights about the mobile part of the phenolic resin (pluronic F127 template). The MAS-DEC spectra are shown in Fig. 9b, and it can be seen that the peaks from 74, 76 ppm corresponding to the carbons in the hydrophobic PPO, are similar for all pH synthesized materials. On the contrary, the peak at 71 ppm related to the carbon in the hydrophilic PEO fragments ($\text{CH}_2\text{-O-CH}_2$) is increasing with the increase of the pH. The PEO/PPO area ratio increases with the pH and is higher than the pure Pluronic template one. This may suggest on one hand the formation of other supplementary species containing C-O-C groups for instance due to reaction between the trihydroxy phenylacetic acid and the glyoxylic acid or between two trihydroxy phenylacetic acid structures as proposed in Eq. (3). On the other hand, this result

implies a faster polymerization rate with the pH increase, in good agreement with the CP-MAS spectra. However, we noticed that pH-5 behaves differently probably due to the fact that polymerization reactions are not favored for pH-5, but rather in basic or acidic conditions.

Further insights on the chemical structure of these phenolic resins were assessed by ^1H NMR (Fig. 10a, b). Two NMR signals are noticed at 3.3 ppm and 1.1 ppm, respectively, corresponding to protons in the ethylene oxides of PEO and propylene oxide of PPO moiety of the F127 surfactant [42]. In addition, for pH-9, a peak at 4.4 ppm is observed which was attributed to cations solvated by water (or “water structure”). In basic conditions, neutralization reaction between the acidic groups and the NaOH may take place giving rise to cations solvated by water [$\text{Na}(\text{H}_2\text{O})_n$]. Other origin of water structures may be the dehydration of PEO moieties in the presence of NaOH [43]. A competition between the K^+ and Na^+ cations for water sites may occur in such conditions.

Regarding the peak placed at 1.1 ppm (H in PPO), a shift to lower frequency (~ 11 Hz) is noticed for pH-5 and pH-9. This may be attributed to an aromatic ring current effect [44]. This suggests proximity of the hydrophobic PPO part of pluronic template with the aromatic planes the phenolic resin. In the case of pH-5 and pH-9 the phenolic resin is more cross-linked as determined by ^{13}C NMR, therefore, more aromatic sites are available.

The interactions between the phenolic resin and the template were studied by ^1H NMR at low fields. Fig. S7 (Supporting Informations) depicts the T1 relaxation curves for phenolic resins obtained using different pH. Based on their behavior, the materials are separated into two groups, pH-1, pH-3 and pH-5, pH-9. The fit of these curves allows to distinguish a mono-component system for pH-1 and pH-3 materials ($A1 = 100\%$), while for pH-5 and pH-9 phenolic resins a bi-component system is determined (Table 3).

Consequently, for pH-1 and pH-3, one relaxation time is obtained (T1,1), indicating intimate interactions between the phenolic resin and the template. For instance, the self-assembly through H-bonding between the oxygen of PPO and PEO segments of pluronic and $-\text{OH}$ or $-\text{COOH}$ groups of phenolic resin may be accounted for such behavior.

In the case of pH-5 and pH-9, two T1 are determined suggesting a bi-component system. The values for spin-lattice relaxation time, T1,1 decrease from 47.9 to 36.3 ms with the increase of the pH from 1 to 9 (Table 3). In addition, for pH-5 and pH-9, a supplementary T1 is determined, i.e., the spin-spin relaxation time (T1,2): 90.6 and 120.3 ms, which is significantly much higher than T1,1 (38.4 and 36.3 ms).

If T1,2 values are compared with those of pure pluronic F127 template, it can be seen that the T1,2 of pluronic is very closed to T1,2 of pH-5 and pH-9 which allow to attribute the A2 fraction to pluronic. This suggests that the pluronic template in the pH-5 and pH-9 resins acts as a “free”, therefore, a “separation” of the phenolic resins and the pluronic template occurred in such conditions explaining the loss of the auto-assembly and mesoporosity, in good agreement with the SAXS results.

To understand this “separation” between the phenol-resin and the template, the effects of salts and NaOH must be considered. The structure of PEO-PPO-PEO block copolymer micelles is described by a core-corona model, in which a spherical core is composed of PPO moieties surrounded by a corona of PEO strongly hydrated by water molecules [48]. The transformation of spherical micelles into worm-like micelles in the presence of KCl have been reported and explained by the dehydration of the PEO chains in the micelle corona [49] due to the increase of the water “structures” [43]. Water structure formation for pH-9 materials have been demonstrated by ^1H NMR spectra (Fig. 10a). The self-assembly process and the organization of the micelles are particularly affected by the

Table 3
¹H NMR relaxation parameters of phenolic resins obtained using different pH.

Materials	A1 (%)	T1,1 (ms)	A2 (%)	T1,2 (ms)
pH-1	100	47.9	–	–
pH-3	100	44.9	–	–
pH-5	34	38.4	66	90.6
pH-9	54	36.3	46	120.3
Pluronic F-127	4.7	0.057	95.3	104.1

A1-fraction component 1; A2-fraction component 2; T1,1 and T1,2-spin-lattice relaxation times.

anions which have stronger influence than the cations [50–54]. For pH-5 and pH-9, the presence of both Cl[−] and HO[−] anions in the reaction mixture lower the cloud point of the PEO chains and the critical micellization temperature [50,51], therefore, the solubility of phenolic-resin decrease (salting-out phenomena), hence they cross-link and precipitate faster. These modifications may trigger different interactions between the micelle corona and the phenolic-resin polymer and *in-fine* various organization of carbon materials [55]. According to the Hofmeister series and the salting-out strength, the anions used here have the following order HO[−] ≫ Cl[−] [51,56]. Therefore, for high pH, dehydration of PEO micelles is induced by NaOH which significantly reduces the H-bonding interactions and self-assembly between the micelles corona and the polymer. This explains the “separation” of phenolic resin and template and the lost of mesoporosity.

4. Discussions

The soft-template approach was combined with the salt template one in order to improve the microporosity of mesoporous carbons. The synthesis conditions allowing to obtain mesoporous materials were inspired from our previous works [13], while in this work the influence of addition of various metallic salts under different experimental conditions was investigated. For pH-1, the nitrogen adsorption/desorption isotherms (Fig. 1) showed no improvement of microporosity by incorporation of KCl salt in the classical reaction mixture (pH-1 NS), however, the mesoporosity was affected. Such result suggests the location of KCl metal salt rather in the proximity of template micelles than in the structure of phenolic resin.

The addition of NaOH increases the pH and induces significant modifications of carbon textural and structural characteristics. When raising the pH up to 5, the microporosity increases then slightly decreases for higher pH (pH-9), while the mesoporosity is gradually lost. The morphology changes (Fig. 2) as well with the pH, from an ordered mesoporous one (pH-1) to a worm-like mesoporous (pH-5), a smooth microporous one (pH-5) and finally to a graphitic-like structure (pH-9).

To explain the textural and morphology evolution with the pH, several analysis were conducted on the phenolic resins before carbonization. SAXS analysis (Fig. 8) demonstrated an ordered mesoporous structure of the phenolic resin prepared at pH-1 which is gradually lost with the increase of the pH up to 9. The ¹H NMR relaxation studies showed only a T1 (Table 3) for pH-1 and pH-3, hence a homogenous monocomponent system composed by the

phenolic resin self-assembled with the template *via* H-bonding interactions is formed. For pH-5 and pH-9, the materials presented two T1, which were associated with a bi-component system, composed of phenolic resin and the pluronic template with limited H-bonding interactions due to the dehydration of PEO segments in basic conditions. These results explain the lost of the mesoporosity with the increase in the pH. For such high pH, the presence of pluronic template is not even required, their textural characteristics being similar as those obtained in the absence of the template (Fig. 7). The graphitization maybe explained by the higher NaOH quantities inducing better cross-linking and stronger synergetic effects between the NaOH and/or KCl and the phenolic resin/template composite.

To understand the development of the microporosity with the increase of pH (amount of NaOH), ¹³C and ¹H NMR (Figs. 9 and 10) was employed. Based on the identification of ¹³C peaks, several reactions pathway mechanisms have been proposed (Eqs. (1)–(3)). Mainly condensation and electrophilic aromatic substitution reactions between the phloroglucinol and glyoxylic acid and/or their derivatives take place which leads to the formation of larger polymer molecules where the phloroglucinol aromatic rings are bridged by lactone or ether groups. The increase of the pH favors the formation of highly substituted phloroglucinol molecules and therefore better cross-linking of phenolic resin. In addition, the ¹H spectra NMR (Fig. 10a) evidenced in the case of pH-9 the formation of cations solvated by water (water structures).

The metallic salt and the NaOH may both play a role on the porosity and on the structural carbon characteristics. The metallic salt act as a porogen, the formation of microporosity being favorised by its dissolution in the carbon network [25,26]. The mechanism is related to dehydration of carbon (removal of oxygen and hydrogen) with the formation of water which leads to pores creation and aromatization of carbon skeleton [57]. When the temperature is increasing the interaction between the carbon and the salt are stronger and the microporosity is significantly improved (Fig. 6). In addition, for higher temperatures than the melting point of the salts, evaporation of metal salt occurs (TGA results, Fig. S8) leading to the development of the mesoporosity as well. LiCl has the lowest melting point (615 °C), higher quantities of LiCl are evaporated (Fig. S8) and it results in the highest mesoporous volume (Table 2).

The base, NaOH also interact with the carbon walls and removes atoms from its lattice and pores may be formed by evolvment of gases such as CO_x [58].

These two separated mechanism scenarios (salt or base) cannot explain the larger surface areas of carbon materials prepared with pH > 3 (between 911 and 1673 m² g^{−1}). If we consider that the materials synthesized only in the presence of KCl salt (pH-1 material) or only in the presence of NaOH (No salt material) have lower surface area (538 and 109 m² g^{−1}, respectively), only synergistic effects between the KCl and NaOH may be accounted for the improvement of microporosity and of the SSA at high pH.

To explain this synergetic effect, the competition between the salt cation (K) and base cation (Na) for water and aromatic sites in the reaction mixture must be analyzed. The hydration enthalpy of the metals varies in the following way: Li > Na > K (Table 4) which

Table 4
 Properties of metals and metal salts [45–47].

Cation	Ionic radius, Å	Hydration enthalpy −ΔH, Kcal/mol	Binding energy −ΔH, Kcal/mol	Melting point metal chlorides, °C
Li	0.60	122	38	615
Na	0.95	98	28	801
K	1.33	77	19	770

allows to assume that in the KCl system, Na^+ will be preferentially hydrated by the water molecules compared to K^+ . However, the mechanism is more complex due to the presence of aromatic molecules in our system (phloroglucinol derived compounds). Such aromatic molecules are known to affect the affinity of the cations vs. water, the cations being more attracted by aromatic molecules than by water through the so called cation- π interactions [45,47,59–61]. It has been shown that in aqueous solution, the K^+ exhibits significantly higher cation- π binding energies than Na^+ and Li^+ [45,47]. This was explained by the fact that the Li and Na have high cation- π binding energies and high solvation energies (Table 4) which induces high desolvation energy of Li and Na to bind further to the benzene ring. Hence, it can be proposed that the K^+ ions are directed mainly towards aromatic rings of phloroglucinol or their substituted derivatives, while the Na^+ ions are more susceptible to hydration by water molecules. Therefore, in the presence of NaOH (pH > 3) the KCl is directed towards the phenolic resin “assuming” its role as microporous template while the NaOH is more directed to the micelles influencing the mesoporosity. As other synthesis were performed also in the presence NaCl or LiCl salts, an order of metal binding to the aromatic rings in aqueous solutions containing NaOH can be proposed: $\text{KCl} > \text{NaCl} > \text{LiCl}$ [45,47].

The salt type influences as well the textural features of the obtained carbons. The surface area and the microporosity increases in the following order, $\text{KCl} > \text{NaCl} > \text{LiCl}$, same order as the binding energies in aqueous medium, while the mesoporosity varies in an opposite manner (Table 2). As proposed by other authors [62], the order of increase in the microporosity maybe also linked with the cation size, i.e., the larger the cation size the higher the surface area. In this work the cation size varies in the following order $\text{K} > \text{Na} > \text{Li}$ (Table 4), therefore in the same way as the SSA (Table 2).

The type of salt induces also alteration of carbon structure (Figs. 4 and 5). The KCl derived carbon presents no graphitic domain (Figs. 4b and 5), while for NaCl and LiCl small graphitic domains are observed (Figs. 4c–f and 5). As report previously [63,64], the thermal treatment of metal/carbon mixtures above the melting point of metal may induce the formation of graphitic nanostructures. This was clearly observed on LiCl which have low melting point (615 °C, Table 4) compared to KCl (790 °C) and which graphitized at lower temperatures (750 °C). Therefore, the graphitization/nanostructuring order varies in the same way as the gas binding energy for cation- π interactions (Table 4), $\text{Li} > \text{Na} > \text{K}$ and inversely to the melting point.

5. Conclusions

Porous carbon materials with various textural and structural characteristics were prepared by a novel soft-salt template synthesis approach and their synthesis mechanism addressed. Various parameters were tuned and their influence on the phenolic resin and carbon characteristics was studied in detail. The increase of reaction mixture pH using NaOH, induces textural and structural modifications. For pH up to 5, a significant improvement in the carbon microporosity but in the detrimental of mesoporosity is obtained. This is accompanied by a morphology change, from mesoporous ordered (pH-1) to worm-like structure (pH-3) and smooth one (pH-5). The ^{13}C and ^1H NMR suggest that the mesoporosity lost is caused by the decrease of H-bonding and self-assembly between the phenolic resin and the template via the formation of water structures by dehydration of template PEO moieties due to the strong “salting-out” effect of $-\text{OH}$ ions. For higher pH (pH-9) the porosity start to decrease and graphene-sheet like morphology is formed.

In addition, several salts were studied (KCl, NaCl and LiCl) and

proved to have different impact on the carbon textural properties and graphitization. The microporous volume and the surface area varies in the following order ($\text{K} > \text{Na} > \text{Li}$) while the mesoporosity in the opposite way. This trend was explained by a synergetic effect between the salt cations and the Na cation for water and aromatic site but also by the metal salt properties.

The structure changes as well from smooth turbostatic (KCl) to defective graphene-sheet like morphology (NaCl, LiCl). The graphitic-like structure formation was explained by the gas-phase binding energies of cations with the aromatic ring which strongly depends on the cation type ($\text{Li} > \text{Na} > \text{K}$).

Acknowledgements

This work was financially supported by the “Pôle Matériaux et Nanoscience d’Alsace-2013”-France. The authors acknowledge Loïc Vidal, Gautier Schroedj and Jean-Marc Le Meins for their assistance with the TEM, ATG and SAXS analysis.

Appendix A. Supplementary data

Supplementary data related to this article can be found at <http://dx.doi.org/10.1016/j.carbon.2016.08.011>.

References

- [1] S. Candelaria, Y. Shao, W. Zhou, X. Li, J. Xiao, J. Zhang, Y. Wang, J. Liu, J. Li, G. Cao, Nanostructured carbon for energy storage and conversion, *Nano Energy* 1 (2012) 195–220.
- [2] J.C. Ndamaniha, L.P. Guo, Ordered mesoporous carbon for electrochemical sensing: a review, *Anal. Chim. Acta* 747 (2012) 19–28.
- [3] J. Tang, J. Liu, N. Torad, T. Kimura, Y. Yamauchi, Tailored design of functional nanoporous carbon materials toward fuel cell applications, *Nano Today* 9 (2014) 305–323.
- [4] W. Xin, Y. Song, Mesoporous carbons: recent advances in synthesis and typical applications, *RSC Adv.* 5 (2015) 83239–83285.
- [5] B. Yuan, X. Wu, Y. Chen, J. Huang, H. Luo, S. Deng, Adsorption of CO_2 , CH_4 , and N_2 on ordered mesoporous carbon: approach for greenhouse gases capture and biogas upgrading, *Environ. Sci. Technol.* 47 (2013) 5474–5480.
- [6] X. Yuan, S.-P. Zhuo, W. Xing, H.-Y. Cui, X.-D. Dai, X.-M. Liu, Z.-F. Yan, Aqueous dye adsorption on ordered mesoporous carbons, *J. Colloid Interface Sci.* 310 (2007) 83–89.
- [7] T. Kyotani, N. Snobe, A. Tomita, Formation of highly orientated graphite from polyacrylonitrile by using a two-dimensional space between montmorillonite lamellae, *Nature* 331 (1988) 331–333.
- [8] J. Lee, S. Han, T. Hyeon, Synthesis of new nanoporous carbon materials using nanostructured silica materials as templates, *J. Mater. Chem.* 14 (2004) 478–486.
- [9] R. Ryoo, S.H. Joo, S. Jun, Synthesis of highly ordered carbon molecular sieves via template-mediated structural transformation, *J. Phys. Chem. B* 103 (1999) 7743–7746.
- [10] L. Chuenchom, R. Kraehnert, B.M. Smarsly, Recent progress in soft-templating of porous carbon materials, *Soft Matter* 8 (2012) 10801–10812.
- [11] T.-Y. Ma, L. Liu, Z.-Y. Yuan, Direct synthesis of ordered mesoporous carbons, *Chem. Soc. Rev.* 42 (2013) 3977–4003.
- [12] Y. Meng, D. Gu, F. Zhang, Y. Shi, H. Yang, Z. Li, C. Yu, B. Tu, D. Zhao, Ordered mesoporous polymers and homologous carbon frameworks: amphiphilic surfactant templating and direct transformation, *Angew. Chem. Int. Ed.* 117 (2005) 7215–7221.
- [13] C. Matei Ghimbeu, L. Vidal, L. Delmotte, J.-M. Le Meins, C. Vix-Guterl, Catalyst-free soft-template synthesis of ordered mesoporous carbon tailored by phloroglucinol/glyoxylic acid environmentally friendly precursors, *Green Chem.* 16 (2014) 3079–3088.
- [14] M. Xie, H. Dong, D. Zhang, X. Guo, W. Ding, Simple synthesis of highly ordered mesoporous carbon by self-assembly of phenol-formaldehyde and block copolymers under designed aqueous basic/acidic conditions, *Carbon* 49 (2011) 2459–2464.
- [15] D. Long, W. Qiao, L. Zhan, L. Liang, Effect of template and precursor chemistry on pore architectures of triblock copolymer-templated mesoporous carbons, *Microporous Mesoporous Mater.* 121 (2009) 58–66.
- [16] S. Tanaka, A. Doi, N. Nakatani, Y. Katayama, Y. Miyake, Synthesis of ordered mesoporous carbon films, powders, and fibers by direct triblock-copolymer-templating method using an ethanol/water system, *Carbon* 47 (2009) 2688–2698.
- [17] Y. Huang, H. Cai, T. Yu, X. Sun, D. Zhao, Highly ordered mesoporous carbonaceous frameworks from a template of a mixed amphiphilic triblock-copolymer system of PEO-PPO-PEO and reverse PPO-PEO-PPO, *Chem. Asian*

- J. 2 (2007) 1282–1289.
- [18] Y. Huang, H. Cai, T. Yu, F. Zhang, Y. Meng, D. Gu, Y. Wan, X. Sun, B. Tu, D. Zhao, Formation of mesoporous carbon with a face-centered-cubic Fd3m structure and bimodal architectural pores from the reverse amphiphilic triblock copolymer PPO-PEO-PPO, *Angew. Chem. Int. Ed.* 46 (2007) 1089–1093.
- [19] M. Enterra, F. Garcia-Suarez, A. Martinez-Alonso, J. Tascon, Avoiding structure degradation during activation of ordered mesoporous carbons, *Carbon* 50 (2012) 3826–3835.
- [20] J. Gorka, A. Zawislak, J. Choma, M. Jaroniec, KOH activation of mesoporous carbons obtained by soft-templating, *Carbon* 46 (2008) 1159–1161.
- [21] J. Zhang, Y. Deng, J. Wei, Z. Sun, D. Gu, H. Bongard, C. Liu, H. Wu, B. Tu, F. Schuth, D. Zhao, Design of amphiphilic ABC triblock copolymer for templating synthesis of large-pore ordered mesoporous carbons with tunable pore wall thickness, *Chem. Mater.* 21 (2009) 3996–4005.
- [22] Y. Li, J. Wei, W. Luo, C. Wang, W. Li, S. Feng, Q. Yue, M. Wang, A. Elzathry, Y. Deng, D. Zhao, Tricomponent coassembly approach to synthesize ordered mesoporous carbon/silica nanocomposites and their derivative mesoporous silicas with dual porosities, *Chem. Mater.* 26 (2014) 2438–2444.
- [23] P. Tripathi, M. Liu, L. Gan, J. Qian, Z. Xu, D. Zhu, N.N. Rao, High surface area ordered mesoporous carbon for high-level removal of rhodamine B, *J. Mater. Sci.* 48 (2013) 8003–8013.
- [24] J. Gorka, M. Jaroniec, Hierarchically porous phenolic resin-based carbons obtained by block copolymer-colloidal silica templating and post-synthesis activation with carbon dioxide and water vapor, *Carbon* 9 (2011) 154–160.
- [25] N. Fechner, T.-P. Fellinger, M. Antonietti, "Salt Templating": a simple and sustainable pathway toward highly porous functional carbons from ionic liquids, *Adv. Mater.* 25 (2013) 75–79.
- [26] E. Masika, R. Mokaya, High surface area metal salt templated carbon aerogels via a simple subcritical drying route: preparation and CO₂ uptake properties, *RSC Adv.* 3 (2013) 17677–17681.
- [27] N. Bhandari, R. Dua, L. Estevez, R. Sahore, E. Giannelis, A combined salt-hard templating approach for synthesis of multi-modal porous carbons used for probing the simultaneous effects of porosity and electrode engineering on EDLC performance, *Carbon* 87 (2015) 29–43.
- [28] X. Deng, B. Zhao, L. Zhu, Z. Shao, Molten salt synthesis of nitrogen-doped carbon with hierarchical pore structures for use as high-performance electrodes in supercapacitors, *Carbon* 93 (2015) 48–58.
- [29] N. Fechner, S.-A. Wohngemuth, P. Jaker, M. Antonietti, Salt and Sugar: direct synthesis of high surface area carbon materials at low temperatures via hydrothermal carbonization of glucose under hypersaline conditions, *J. Mater. Chem. A* 1 (2013) 9418–9421.
- [30] J. Ludwinowicz, M. Jaroniec, Potassium salt-assisted synthesis of highly microporous carbon spheres for CO₂ adsorption, *Carbon* 82 (2015) 297–303.
- [31] L. Roldan, Y. Marco, E. Garcia-Bordeje, Bio-sourced mesoporous carbon doped with heteroatoms (N,S) synthesized using one-step hydrothermal process for water remediation, *Micro. Mesoporous. Mater.* 222 (2016) 55–62.
- [32] S. Zhu, J. Li, C. He, N. Zhao, E. Liu, C. Shi, M. Zhang, Soluble salt self-assembly-assisted synthesis of three-dimensional hierarchical porous carbon networks for supercapacitors, *J. Mater. Chem. A* 3 (2015) 22266–22273.
- [33] J. Jagiello, J. Olivier, Carbon slit pore model incorporating surface energetical heterogeneity and geometrical corrugation, *Adsorption* 19 (2013) 777–783.
- [34] J. Jagiello, J. Olivier, 2D-NLDFT adsorption models for carbon slit-shaped pores with surface energetical heterogeneity and geometrical corrugation, *Carbon* 55 (2013) 70–80.
- [35] M. Pimenta, G. Dresselhaus, M. Dresselhaus, L. Cancado, A. Jorio, R. Saito, Studying disorder in graphite-based systems by Raman spectroscopy, *Phys. Chem. Chem. Phys.* 9 (2007) 1276–1290.
- [36] A.C. Ferrari, Raman spectroscopy of graphene and graphite: disorder, electron-phonon coupling, doping and nonadiabatic effects, *Solid State Commun.* 143 (2007) 47–57.
- [37] A. Ahmed, Methanol effect on color stability and shelf life of phenolic resin compound under acidic conditions, *Iraqi J. Chem. Pet. Eng.* 10 (2007) 57–63.
- [38] Y. Ito, N. Sugimoto, T. Akiyama, T. Yamazaki, K. Tanamoto, Cepaic acid, a novel yellow xanthylum pigment from the dried outer scales of the yellow onion *Allium cepa*, *Tetrahedron Lett.* 50 (2009) 4084–4086.
- [39] Y. Meng, D. Gu, F. Zhang, Y. Shi, L. Cheng, D. Feng, Z. Wu, Z. Chen, Y. Wan, A. Stein, D. Zhao, A family of highly ordered mesoporous polymer resin and carbon structures from organic-organic self-assembly, *Chem. Mater.* 18 (2006) 4447–4464.
- [40] F. Zhang, Y. Meng, D. Gu, Y. Yan, Z. Chen, T. Bo, D. Zhao, An aqueous cooperative assembly route to synthesize ordered mesoporous carbons with controlled structures and morphology, *Chem. Mater.* 18 (2006) 5279–5288.
- [41] O. Han, Y. Bae, Solid-state NMR study on the structure and dynamics of triblock copolymers P123 remaining in SBA-15 after solvent washing, *Bull. Korean Chem. Soc.* 29 (2008) 911–912.
- [42] E. Rampazzo, R. Voltan, L. Petrizza, N. Zaccaroni, L. Prodi, F. Casciano, G. Zauli, P. Secchiero, Proper design of silica nanoparticles combine high brightness, lack of cytotoxicity and efficient cell endocytosis, *Nanoscale* 5 (2013) 7897–7905.
- [43] E. Florin, R. Kjellander, J. Eriksson, Salt effects on the cloud point of the poly(ethylene oxide)+ water system, *J. Chem. Soc. Faraday Trans. 1* 80 (1984) 2889–2910.
- [44] A. Forse, J. Griffin, V. Presser, Y. Gogotsi, C. Grey, Ring current effects: factors affecting the NMR chemical shift of molecules adsorbed on porous carbons, *J. Phys. Chem. C* 118 (2014) 7508–7514.
- [45] R. Kumpf, D. Dougherty, A mechanism for ion selectivity in potassium channels: computational studies of cation- π interactions, *Science* 261 (1993) 1708–1710.
- [46] A. Stace, Estimating the hydration enthalpies of neutral alkali metal atoms, *J. Phys. Chem.* 110 (2006) 20742–20744.
- [47] D. Dougherty, The cation- π interaction, *Acc. Chem. Res.* 46 (2013) 885–893.
- [48] P. Alexandridis, V. Athanassiou, S. Fukuda, T. Hatton, Surface activity of poly(ethylene oxide)-block-poly(propylene oxide)-block-poly(ethylene oxide) copolymers, *Langmuir* 10 (1994) 2604–2612.
- [49] H. Heerklotz, A. Tsamaloukas, K. Kita-Tokarczyk, P. Strunz, T. Gutberlet, Structural, volumetric, and thermodynamic characterization of a micellar sphere-to-rod transition, *J. Am. Chem. Soc.* 126 (2004) 16544–16552.
- [50] P. Alexandridis, J. Holzwarth, Differential scanning calorimetry investigation of the effect of salts on aqueous solution properties of an amphiphilic block copolymer (poloxamer), *Langmuir* 13 (1997) 6074–6082.
- [51] E. Leontidis, Hofmeister anion effects on surfactant self-assembly and the formation of mesoporous solids, *Curr. Opin. Colloid & Interface Sci.* 7 (2002) 81–91.
- [52] C. Matei Ghimbeu, J. Le Meins, C. Zlotea, L. Vidal, G. Schroedj, M. Latroche, C. Vix-Guterl, Controlled synthesis of NiCo nanoalloys embedded in ordered porous carbon by a novel soft-template strategy, *Carbon* 67 (2014) 260–272.
- [53] S. Sun, C. Matei Ghimbeu, R. Janot, J.M. Le Meins, A. Cassel, C. Davoisne, C. Masquelier, C. Vix-Guterl, One-pot synthesis of LiFePO₄-carbon mesoporous composites for Li-ion batteries, *Microporous Mesoporous Mater.* 198 (2014) 175–184.
- [54] D. Zhao, Q. Huo, J. Feng, B. Chmelka, G. Stucky, Non-ionic triblock and star diblock copolymer and oligomeric surfactant syntheses of highly ordered, hydrothermally stable, mesoporous silica structures, *J. Am. Chem. Soc.* 120 (1998) 6024–6036.
- [55] S. Schlienger, C. Ducrot-Boisgontier, L. Delmotte, J.-L. Guth, J. Parmentier, History of the micelles: a key parameter for the formation mechanism of ordered mesoporous carbons via a polymerized mesophase, *J. Phys. Chem. C* 118 (2014) 11919–11927.
- [56] W. Kunz, J. Henle, B. Ninham, Zur Lehre von der Wirkung der Salze (about the science of the effect of salts: Franz Hofmeister's historical papers, *Curr. Opin. Colloid Interface Sci.* 9 (2004) 19–37.
- [57] Z. Hu, E.A. Vansant, New composite adsorbent produced by chemical activation of elutriilite with zinc chloride, *J. Colloid Interface Sci.* 176 (1995) 422–431.
- [58] F. Rodriguez-Reinoso, M. Molina-Sabio, Activated carbons from lignocellulosic materials by chemical and/or physical activation: an overview, *Carbon* 30 (1992) 1111–1118.
- [59] J. Sunner, K. Nishizawa, P. Kerbale, Ion-solvent molecule interactions in the gas phase. The potassium ion and benzene, *J. Phys. Chem.* 85 (1981) 1814–1820.
- [60] O. Cabarcos, C. Weinheimer, J. Lisy, Size selectivity by cation- π interactions: solvation of K⁺ and Na⁺ by benzene and water, *J. Chem. Phys.* 110 (1999) 8429–8435.
- [61] O. Cabarcos, C. Weinheimer, C. Lisy, Competitive solvation of K⁺ by benzene and water: cation- π interactions and π -hydrogen bonds, *J. Chem. Phys.* 108 (1998) 5151–5154.
- [62] K. Okada, N. Yamamoto, Y. Kameshima, A. Yasumori, Porous properties of activated carbons from waste newspaper prepared by chemical and physical activation, *J. Colloid Interface Sci.* 262 (2003) 179–193.
- [63] A. Kamali, D. Fray, Molten salt corrosion of graphite as possible way to make carbon nanostructures, *Carbon* 56 (2013) 121–131.
- [64] J. Sure, A. Shankar, S. Ramya, U. Mudali, Molten salt corrosion of high density graphite and partially stabilized zirconia coated high density graphite in molten LiCl-KCl salt, *Ceram. Int.* 38 (2012) 2803–2812.